

# Development of a 3D Printed Loop Heat Pipe

Bradley Richard<sup>1</sup>, Bill Anderson<sup>2</sup>, Chien-Hua Chen<sup>3</sup>, Joel Crawmer<sup>4</sup>, and Merryl Augustine<sup>5</sup>  
*Advanced Cooling Technologies, Inc., Lancaster, PA, 17601*

As the capabilities of CubeSats and SmallSats increase, so do the heat rejection requirements. While loop heat pipes (LHPs) are capable of transporting heat across deployable radiators, they are currently too expensive for most applications. The largest cost comes from the fabrication of the primary wick which requires multiple machining steps as well as a knife-edge seal. The focus of this work is the development of a 3D printed LHP evaporator using a direct metal laser sintering (DMLS) process to fabricate the primary wick. 3D printing of LHP wicks offers several advantages. The overall cost can be significantly reduced by eliminating multiple machining steps, and the risk of failure can be reduced by eliminating the knife-edge seal. The challenge with 3D printing of LHPs is achieving a porous wick structure. A pore radius and permeability study was conducted for optimization of DMLS methods and parameters for fabricating both the primary and secondary wicks. The primary wick and secondary wick were also fabricated as a single part to test the ability to connect areas of varying pore size. Experimental testing was completed on a complete LHP prototype with 3D printed primary wick fabricated using the optimized DMLS parameters. A 3D printed secondary wick has also been developed. Preliminary results show that it is feasible to 3D print the envelope, primary wick, and secondary wick in a single process.

## I. Introduction

NASA's CubeSat and SmallSat programs provide the ability to rapidly develop and launch small-scale satellite platforms for research and technology demonstration purposes, while reducing costs and increasing efficiency. Conventional spacecraft thermal control systems utilize constant conductance heat pipes (CCHPs) and encapsulated pyrolytic graphite for the passive transport of waste heat. However, pyrolytic graphite is very expensive, and CCHPs are difficult to test on the ground and are generally not used for deployable radiators. Loop heat pipes (LHPs) are another commonly utilized thermal control system for spacecraft, but the manufacturing costs are currently too high to make them viable for most CubeSat/SmallSat applications. In this work a low-cost LHP evaporator was fabricated using an additive manufacturing technique called Direct Metal Laser Sintering (DMLS).

DMLS is a process by which metal structures are made in a layer-by-layer sintering process which selectively melts powdered metal. Part geometries should complement the building process, which favors upward slanting surfaces and large radii just under horizontal structures. Utilizing the DMLS process, metal parts of the most complex geometries are built layer-by-layer directly from 3D CAD models. Unique geometric freedom of design enables DMLS to form cavities and undercuts, which may be very difficult, or even impossible, for conventional machining methods to fabricate. In most 3D printing applications, the metal powder is melted entirely to create a fully dense, homogenous structure. However, for an LHP primary wick an intentionally porous part must be printed with a pore radius on the order of 1-10 $\mu\text{m}$  in order to have enough capillary pressure to overcome the total pressure drop of the LHP. A porous part can be fabricated by adjusting the DMLS parameters so that complete melting does not occur, but pore sizes have been limited to  $>50\mu\text{m}$ . In this work a small-scale parameter study optimized DMLS parameters to produce porous wicks with pore radii  $<10\mu\text{m}$ .

The work presented in this paper is on the second-generation 3D printed LHP prototype. The first-generation prototype successfully demonstrated the ability to use DMLS to fabricate a primary wick. However, the pore radius of the primary wick was 44 $\mu\text{m}$  which limited the maximum power before dry-out to only 45W. A more comprehensive

---

<sup>1</sup> R&D Engineer, 1046 New Holland Ave. Lancaster, PA 17601.

<sup>2</sup> Chief Engineer, R&D, 1046 New Holland Ave. Lancaster, PA 17601.

<sup>3</sup> Lead Engineer, R&D, 1046 New Holland Ave. Lancaster, PA 17601.

<sup>4</sup> R&D Engineer, 1046 New Holland Ave. Lancaster, PA 17601.

<sup>5</sup> R&D Intern, 1046 New Holland Ave. Lancaster, PA 17601.

DMLS parameter optimization study to improve performance was conducted. The current pore size of the 3D printed wicks is 6  $\mu\text{m}$ .

## II. Background

### A. Loop Heat Pipe Operation

LHPs are high thermal conductance devices that are self-contained and passive. Figure 1 shows a schematic of an LHP. Note that the figure is not to scale; the vapor and liquid lines can be made much longer. Heat enters the evaporator and vaporizes the working fluid at the interface between the wick and envelope. The vapor is collected by a system of grooves and headers. The vapor flows down the vapor line to the condenser where it condenses as heat is removed by the cold plate. Most of the condenser is filled with a two-phase mixture. A small section at the end of the condenser provides a small amount of liquid sub-cooling.

The compensation chamber (or reservoir) at the end of the evaporator is designed to operate at a lower temperature than the evaporator, although the temperature difference is low for most applications. The temperature of the compensation chamber can be used to control the operating temperature of the LHP. Since the temperature is lower, the pressure of the saturated fluid in the compensation chamber is also lower. This lower pressure draws the condensate through the condenser and the liquid return line<sup>2</sup>. The fluid then flows into a central pipe where it feeds the wick. Excess fluid drains into the compensation chamber. A secondary wick in the evaporator and compensation chamber allows the liquid in the compensation chamber to feed the evaporator wick. This communication between the compensation chamber and primary wick is required during transient operations. The liquid in the compensation chamber and the interior of the wick must be returned to the exterior surface of the wick to close the cycle. Capillary forces accomplish this passively, pulling liquid back to the surface, similar to water being absorbed into a sponge. Loop heat pipes are made self-priming by carefully controlling the volumes of the compensation chamber, condenser, vapor line and liquid line so that liquid is always available to the wick. The compensation chamber size and fluid charge are set so that there is always fluid in the compensation chamber even if the condenser, vapor line and liquid line are completely filled. The LHP is thus inherently self-priming.

### B. Loop Heat Pipe Fabrication

The key component of the Loop Heat Pipe system is the pump assembly, which consists of the evaporator and the compensation chamber<sup>1</sup>. A detailed view of this assembly is shown in Figure 2. The key subcomponents of the pump assembly consist of the cylindrical envelope, a primary wick, a secondary wick, the bayonet, two bi-metallic transition couplings, and the Knife Edge Seal (KES). The compensation chamber is welded to the evaporator subassembly via a bimetallic transition with steel and aluminum sections. The KES is critical for developing the differential pressure required to drive the working fluid around the system. The need for a KES and bi-metallic joints is a large source of the shortcomings associated with LHP evaporator production and reliability.

Currently, the primary wick structure is produced external from the envelope, using sintered Nickel powder. The fabrication process entails compacting Nickel powder into a sintering mandrel and firing at high temperatures. The oversize wick is then machined at low speeds, and without lubricant to produce the vapor grooves and reduce the outer diameter to the proper size while preventing contamination.

Once the primary wick structure is successfully produced, machined to the correct size, and hydrodynamically characterized, the insertion of the wick into the envelope takes place. With a slight interference fit at room temperature between the primary wick and the evaporator body, the envelope must be heated to expand the inner diameter of the envelope. Then the wick is chilled to slightly reduce its diameter and inserted. The design of the wick and the interference fit theoretically results in intimate contact between all the circumferential grooves of the wick and the aluminum envelope. In practice, once the wick is installed the actual contact area is unknown. It is suspected that the

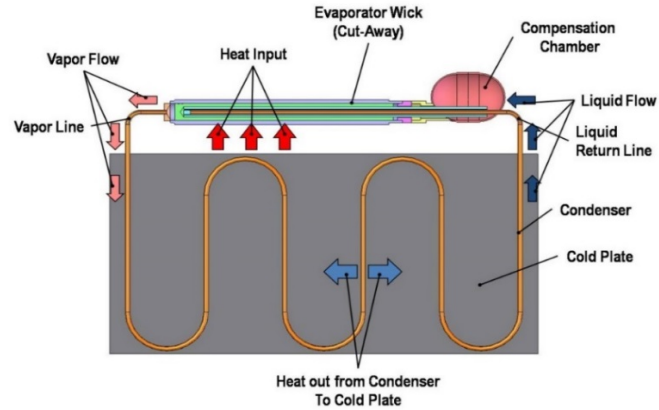
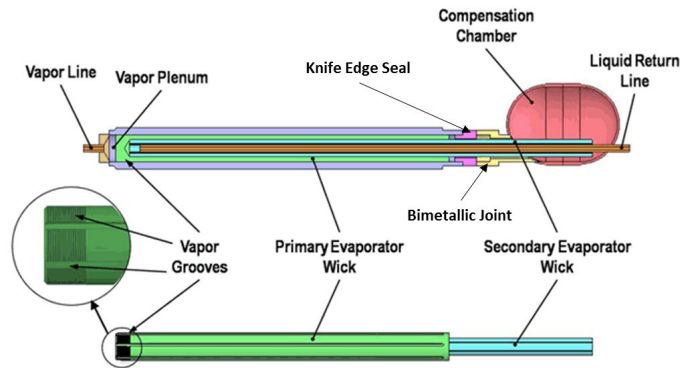


Figure 1. Loop heat pipe schematic (not to scale).

physical insertion of the wick shaves and smears the circumferential grooves thereby reducing contact and subsequently the thermal performance of the assembly.

Once the primary wick structure is inserted into the envelope, the KES must be installed. A bi-metallic insertion piece with the knife edge features is evenly pressed into the sintered wick, creating a seal between the inner and outer regions of the primary wick. A bi-metallic interface is necessary because it is desirable to have a KES material with a higher hardness than the Aluminum LHP envelope in order to maintain the integrity of the KES. Experience has shown that a proper seal is not always achieved, and if this KES insertion process fails and reinsertion is attempted, the primary wick is likely to become damaged. This damage typically requires the wick to be



**Figure 2. Detailed view of LHP evaporator**

scrapped. The envelope may be reused but a new wick must be manufactured. It is also possible for the KES to pass verification testing after assembly but fail later after numerous thermal cycles or vibration testing.

Once the bayonet and secondary wick subassembly are inserted down the bore of the primary wick, the next step in the LHP pump assembly is attaching the front end of the compensation chamber by welding to the bimetallics. This process is of concern, due to mismatches in the material coefficient of thermal expansion (CTE) in the Aluminum-Stainless Steel bimetallic transition coupling. Excessive heating of the coupling causes the materials to expand at different rates resulting in a significant stress at the two-material interface. The bimetallic coupling is an off-the-shelf component, and that interface is produced using a friction-stir welding process that has historically been shown to produce an excellent bond between dissimilar metals. However, excessive heating of this component has an inherent high level of risk and has resulted in part failure.

By utilizing additive manufacturing techniques, the fabrication process for LHPs can be significantly simplified, thereby reducing the risk and cost associated with the traditional manufacturing techniques. Specifically, 3D printing enables the evaporator to be printed as one part, including both the wick structure and envelope. The additional parts of the evaporator assembly, such as the vapor line and compensation chamber, can be welded directly to the evaporator part, eliminating the requirement for a KES.

The development of the 3D printed LHP wick is discussed in a previous paper.<sup>3</sup> Wicks were fabricated with different sintering parameters, and ranked. The best wick had a 6 $\mu$ m pore size. Achieving smaller pore sizes is likely only possible by using smaller diameter metal powder as the base material, but there are no such commercially available powders currently.

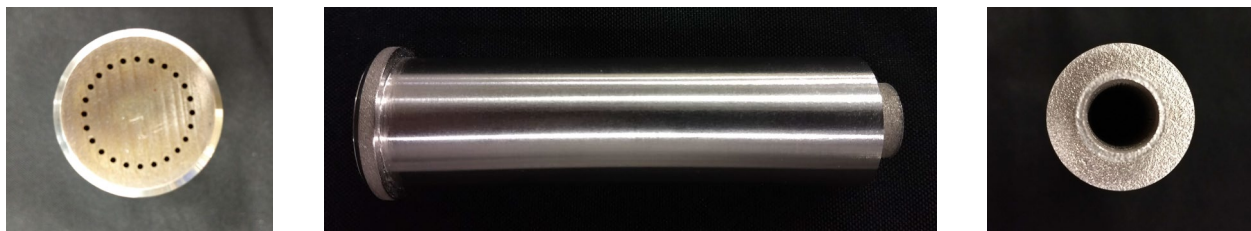


**Figure 3. 3D Printed LHP Evaporator.**

An LHP evaporator was fabricated using the best set of parameters, see Figure 3. The vapor vents, shown in the evaporator front (left), are used to feed the vapor generated in the evaporator to the vapor line. They are formed during the 3D printing process. A cap is welded around the front of the evaporator, forming a vapor plenum that feeds the vapor line. The back of the LHP evaporator is shown at the right of Figure 3. One of the main advantages of the 3D printed LHP evaporator is the elimination of the knife-edge seal, which is usually required to seal the pressure difference between the evaporator exterior and the compensation chamber. In the 3D printed LHP, the printing parameters were just altered to provide a solid cap above the wick.

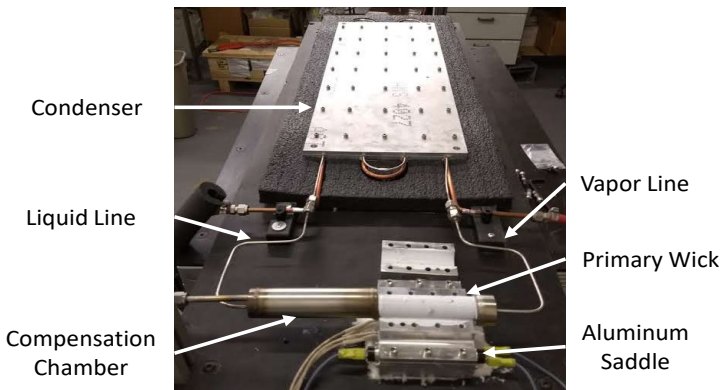


**Figure 4. Completed LHP prototype with 3D printed primary wick.**

A proof of concept LHP prototype was built using this evaporator, as shown in Figure 4. The working fluid used was ammonia. The primary wick was 2.54cm in diameter and 10.2cm in length. The primary wick as printed had a porous interior with a fully dense envelope which was welded directly to the compensation chamber and vapor line. The tubing was 0.318cm in diameter and the condenser was 99cm in length.

Initial testing of the LHP prototype was described in an earlier paper.<sup>3</sup> For a system intended to be used in microgravity, the LHP is generally tested with the evaporator elevated above the condenser, with both

evaporator and condenser horizontal.

For Lunar and Martian Landers and Rovers, LHPs will have to operate with the evaporator tilted in any direction, so flexible lines were installed between the evaporator and the condenser.

### III. Adverse Condition Testing

In order to experimentally test the effect of adverse conditions on the 3D printed LHP performance, flexible lines were installed between the evaporator and condenser of the LHP prototype. First a baseline test was completed on the LHP with flexible lines to detect any change in performance. A plot of the results is shown in Figure 5. Startup was immediate at an input power of 100W. Steady state was then reached at powers of 100 and 110W. At 120W the temperature of the evaporator continued to increase until an over-temp controller interrupted the input power to the test. Previously a maximum power of 125W was reached, but the newly installed flexible lines add to the pressure drop through the liquid and vapor lines and reduce the maximum power capability.

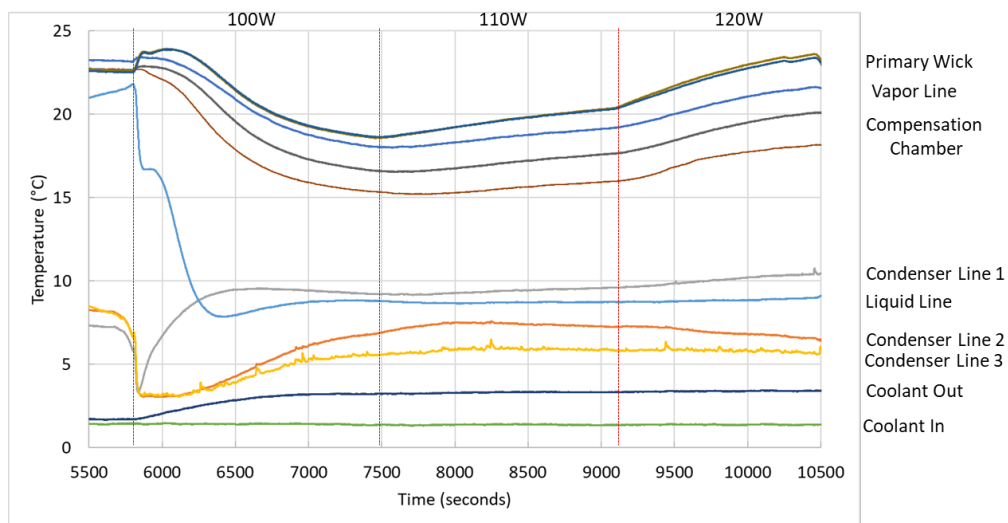


**Figure 5. Baseline testing with flexible lines added to prototype**

Next, steady state testing was completed with the evaporator raised 13.3cm (5.25in.) above the condenser, representing an adverse elevation case. Due to the use of flexible lines, the evaporator and condenser sections of the LHP were able to be held flat during adverse elevation testing. The test results are provided in Figure 6. As with the baseline test, steady state operation was achieved at powers of 100 and 110W. Although, higher temperatures were measured in the evaporator assembly due to the adverse elevation condition.

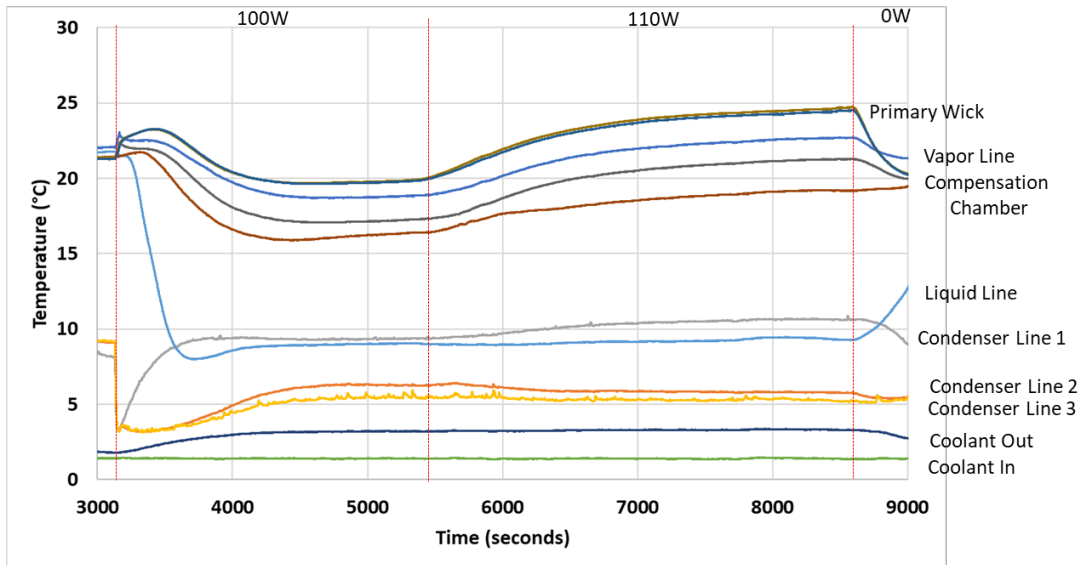


**Figure 6. Steady state testing of prototype at an adverse elevation of 5.25” with both the evaporator and condenser flat**

To test feasibility for Lunar and Martian lander and rover applications the evaporator was then tilted to an adverse angle of 25°, such that the compensation chamber was below the primary wick. A picture of the evaporator tilted at 25°, and the orientation of the evaporator with respect to the condenser is shown in Figure 7. The purpose of testing with a tilted evaporator is to test the ability of the secondary wick to operate against gravity. This is important for any potential lander applications on the moon or Mars where the rover will need to be able to handle uneven terrain. To test the performance of the secondary wick under these conditions the power was cycled between 100 and 50W. During transients, the secondary wick must pump liquid to the primary wick to prevent dry-out. A plot of the results is shown in Figure 8. The primary wick did not dry-out during the power cycling, and steady state was reached at 100 and 50W.



**Figure 7. LHP prototype with flexible lines added to allow for tilting of the evaporator at angles up to 25°**

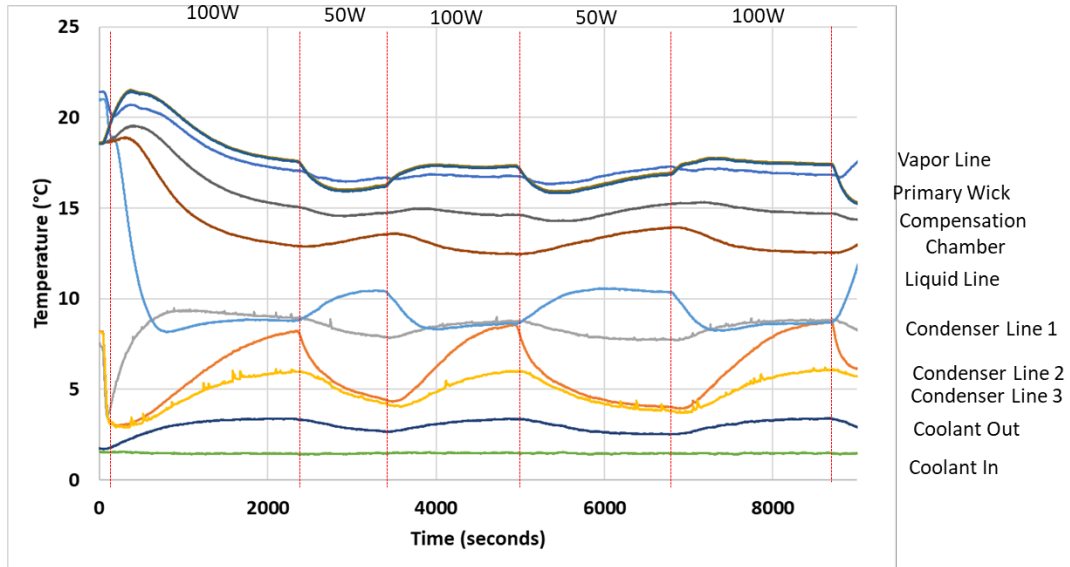


Figure 8. Power cycle testing of prototype with evaporator tilted at 25° against gravity

#### IV. Vibration Loading

The evaporator on the current LHP prototype which had been previously tested was removed from the condenser and prepared for vibration testing as shown in Figure 9. The evaporator was exposed to the vibration profile presented in Table 1 which was taken from previous requirements for satellite launches. The goal of vibration testing is to demonstrate the robustness of the 3D printed primary wick.

Table 1. Vibration loading conditions for the 3D printed evaporator assembly

Random Vibration Spectrum – X and Y Axis		Random Vibration Spectrum – Z Axis	
Frequency (Hz)	$g^2/Hz$	Frequency (Hz)	$g^2/Hz$
20	0.020	20	0.026
50	0.080	50	0.160
800	0.080	800	0.160
2000	0.020	2000	0.026

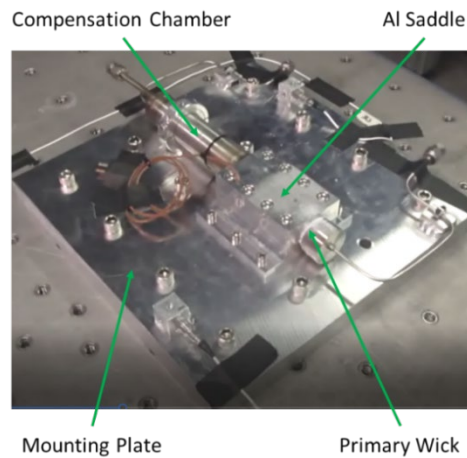
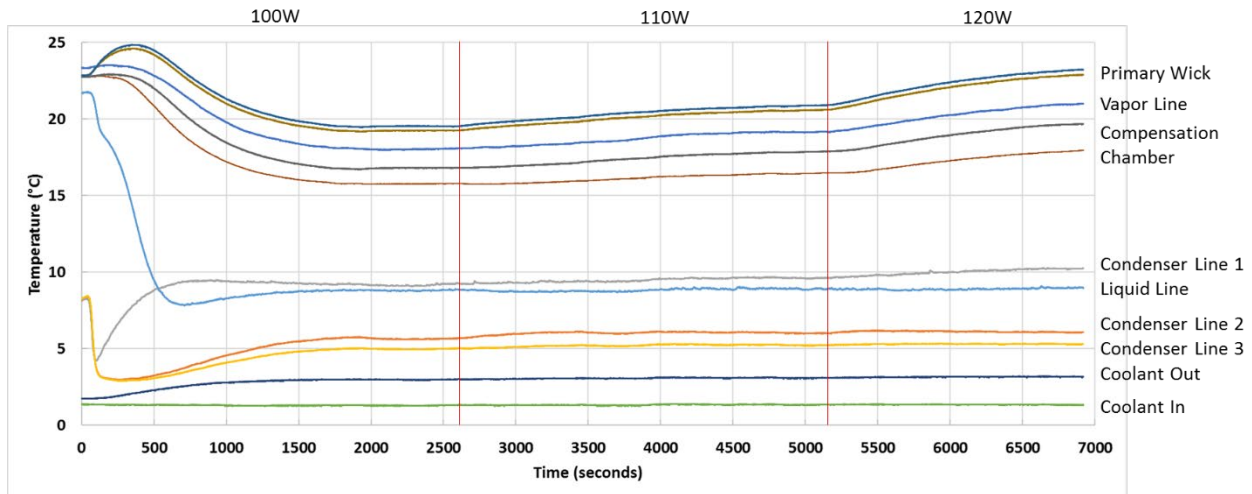


Figure 9. LHP evaporator assembly on vibration table for testing

Steady state testing was completed on the LHP prototype before and after vibration testing to compare performance. A plot of the steady state testing results before vibration testing was previously presented in Figure 5. A plot of the steady state testing results after vibration testing is presented in Figure 8. After vibration testing the prototype successfully reached steady state at powers of 100W and 110W. The operating temperatures of the before and after tests are very similar. These results verify that there was no loss in performance of the LHP after vibration testing which demonstrates that the 3D printed primary wick did not sustain any damage.



**Figure 10. Steady state testing of LHP after vibration testing with flexible lines**

### V. Preliminary Results for 3D Printing Secondary Wicks

The results above demonstrate that the primary wick and envelope can be inexpensively fabricated by 3D printing. As shown in Figure 2 above, the secondary wick is built up around the liquid return line (bayonet) in the evaporator and compensation chamber. It provides additional liquid, if the liquid returning from the condenser is insufficient, e.g., during power transients. The secondary wick is currently built up around the bayonet and sintered separately, and then inserted into the primary wick. 3D printing the secondary wick can significantly reduce costs, particularly if it can be fabricated together with the envelope and primary wick.

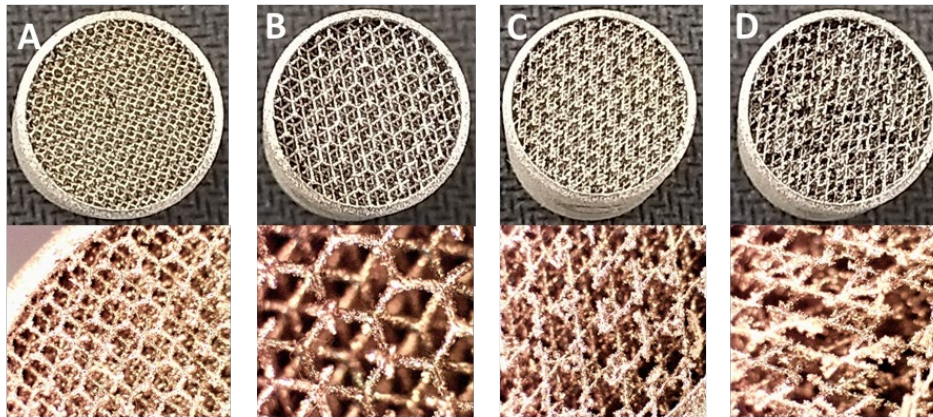


**Figure 11. 3D printed secondary wicks using a defined lattice structure.**

Ideally, the secondary wick should have a pore size around 30-50 $\mu\text{m}$ . Lattice structures were evaluated as a possible method for fabricating the secondary wick. A total of 8 different lattice structures were printed; four of which are shown in Figure 11. The use of a defined lattice structure had several challenges. The large file sizes made creating the structures difficult even for small cylindrical samples. The DMLS machine could not print more than four parts at a time due to challenges with the file size and complexity. Samples E through H were only printed half height due to the machine crashing. Samples A through D had very large pores on the order of 1mm and were brittle with defects.

Based on these results a defined lattice structure does not seem to be a feasible method for printing of full-scale secondary wicks.

Primary and secondary wick samples from a second wick supplier are shown in Figure 12. Both wicks were fabricated by rastering the laser, similar to the primary wick samples from the first supplier. The pore size and permeability of each sample was measured and the results are plotted in Figure 13. For the primary wicks a pore size of 5µm was achieved with a much higher permeability than previous wicks. The higher permeability is due to an increase in porosity. Previous wicks had porosities of 20-24% while the new primary wicks have a porosity of 31%. A coarse wick for the secondary wick was also achieved without the wick becoming brittle or containing defects.

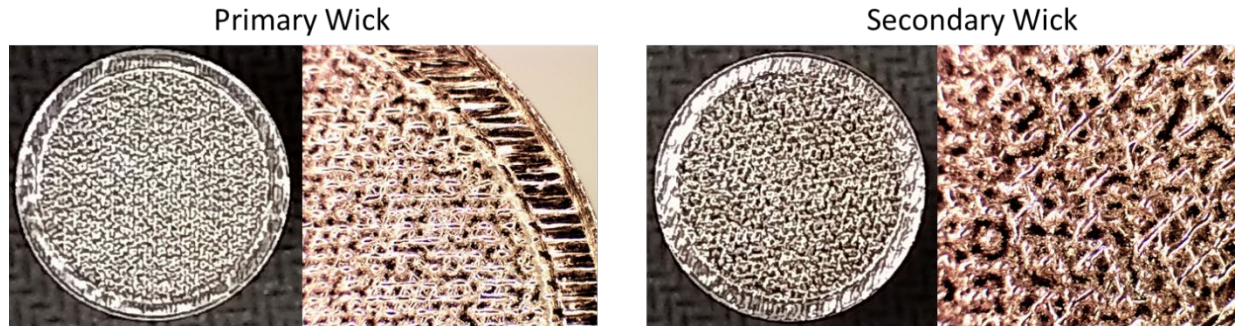


Figure 12. Images of 3D printed wick samples from a second supplier.

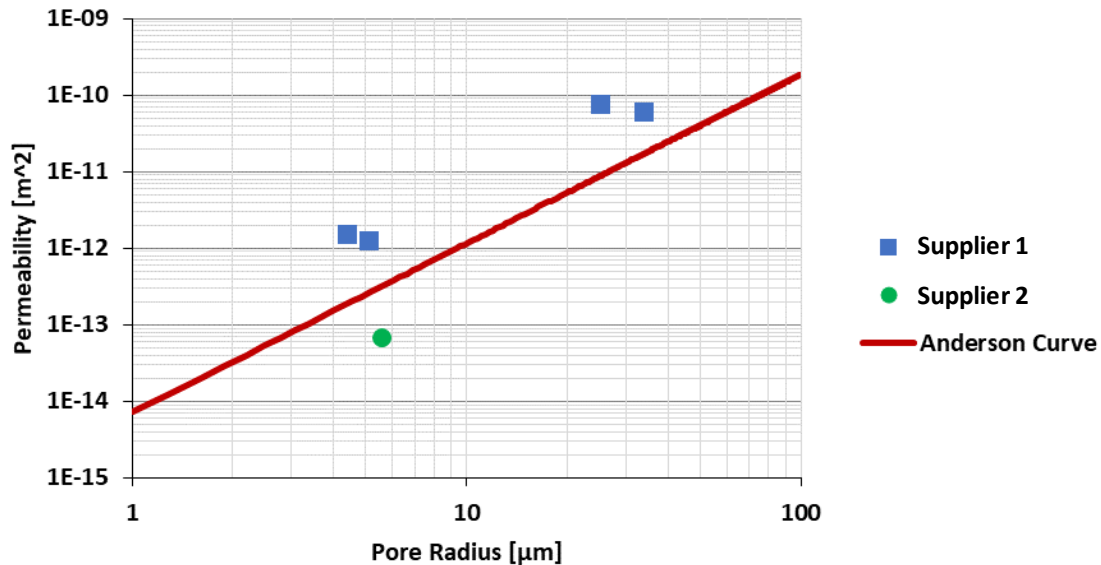


Figure 13. Pore size and permeability testing result of new wick samples demonstrating higher permeabilities than previous wicks

The Anderson curve is a curve fit for pore size versus permeability in sintered wicks, developed by one of the co-authors. It is based on several hundred experimental porosity/permeability measurements on steel, stainless steel, superalloy, nickel, copper, aluminum, and refractory metal wicks:

$$\frac{K}{m^2} = 0.125 \cdot \left( \frac{r_c}{m} \right)^{2.207}$$

The feasibility of using 3D printing to print primary wick and secondary together was initially investigated by building a small test sample (2.54cm diameter x 2.54cm tall, Figure 14 (a)). It is possible that the interface between the two wicks could have a very low permeability, or, on the other hand, gaps. The shape was chosen so that flow from one wick to the other could be verified. The sample was later sectioned to examine the interface in more detail.

The fine wick was printed via the printing parameters for about 5 µm and the coarse wick was printed via the printing parameters for about 30 µm. Figure 14 (b) shows a microscope picture of the cross-section of the 3D printed

bi-porous wick sample. The fine wick, the coarse wick, and the fully dense wall were able to be printed in one piece in a single batch process.

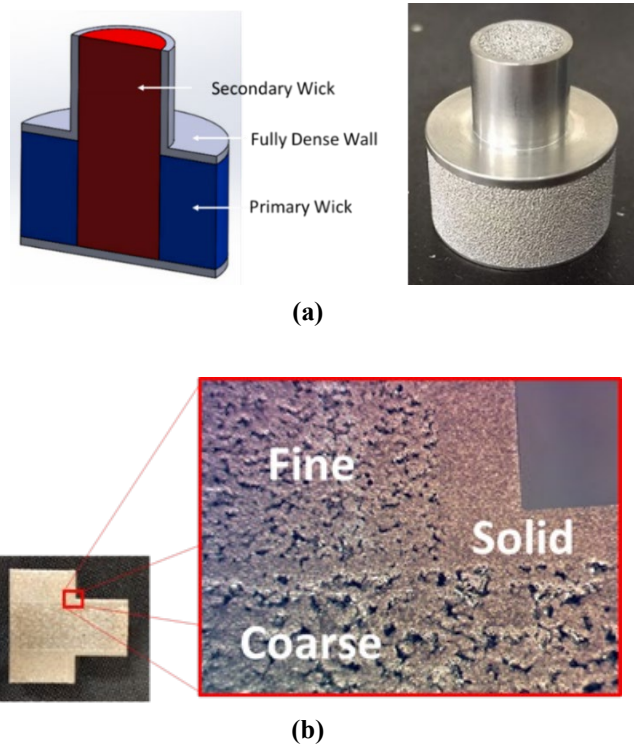


Figure 14. (a) Test sample with combined primary and secondary wicks. (b) Section through a primary/secondary wick sample, showing the interfaces between the two wicks, and between the wicks and solid envelope.

To characterize the printed bi-porous wick, a CFD model was used to estimate the relation between the pressure and the flow flux, and the results were compared to the experimental data. To simplify the calculation, a diffusion model based on the thermal and fluid analogy was used. Figure 15 shows the corresponding terms between the Fourier’s Law and Darcy’s Law. The relation of flow flux and pressure can be obtained by solving the diffusion equation via a commercial CFD package. Figure 16 shows the simulated pressure contour (converted from the temperature contour) of the bi-porous sample.

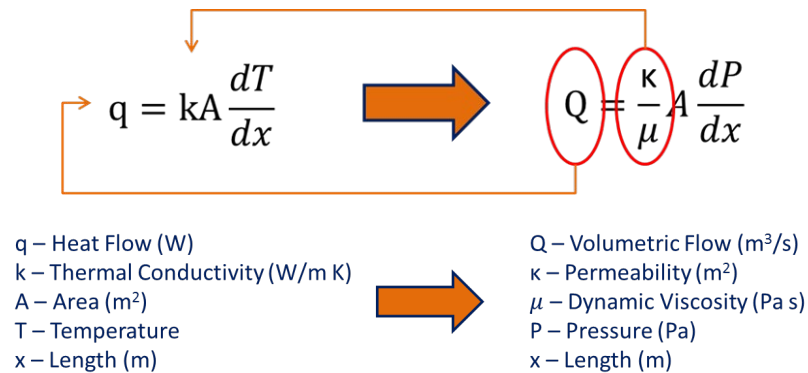


Figure 15. The corresponding terms of thermal (Fourier’s Law) and fluid (Darcy’s Law) analogy.

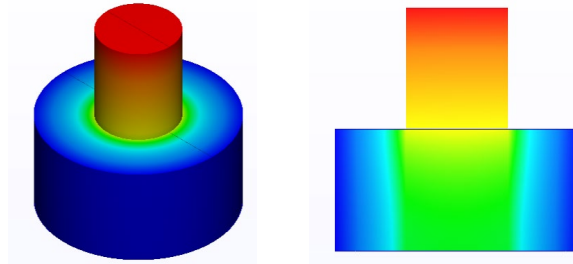


Figure 16. Temperature contour calculated based on Fourier's diffusion law, which can be analogized to the pressure in the Darcy's law.

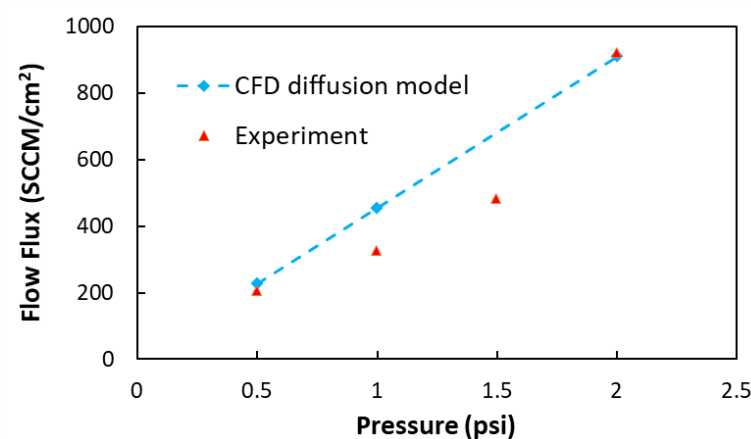


Figure 17. A comparison between experimental measurement and CFD diffusion model of the 3D printed bi-pore size sample.

The experimental pressure drop was determined by applying a constant pressure on the top surface of the secondary wick, and then measuring the flow rate via rotameter. The experimental measurement shows good agreement with the computational result assuming  $5\mu\text{m}$  and  $30\mu\text{m}$  pore sizes (Figure 17), suggesting that no blockage in the interface of the fine and coarse wicks when they are printed simultaneously. The next step is to fabricate the envelope, primary wick, and secondary wick in the standard configuration.

## VI. Conclusion

The performance of 3D printed LHPs is lower than that of conventional systems, but is sufficient for most CubeSat applications. The major benefit is the significant cost reduction, making them affordable for CubeSats, which generally have a lower budget than larger satellites. Significant progress has been made in the development of 3D printed LHP evaporators. These include:

- Testing demonstrated the ability of the 3D printed evaporator to operate against gravity. The evaporator also operated while tilted at an angle of  $25^\circ$  demonstrating feasibility for application on lunar or Martian landers and rovers.
- Vibration testing was completed on the 3D printed primary wick and evaporator assembly. The prototype was shown to be fully operational after vibration testing, verifying the robustness of the 3D printed wick.
- 3D printed secondary wicks were also developed. An initial experiment showed that it should be possible to 3D print the envelope, primary wick, and secondary wick together, further reducing fabrication costs.

Future work consists of 3D printing both primary and secondary wicks as a single part to further reduce fabrication costs and lead times. Additionally, a miniature LHP is being fabricated for a potential flight test.

## Acknowledgments

This work was funded by NASA through the Small Business Innovation Research (SBIR) program under contract NNX17CM09C. The technical monitor is Dr. Jeff Farmer.

## References

<sup>1</sup>Anderson, W.G., Dussinger, P.M., Garner, S.D., Hartenstine, J.R., and Sarraf, D.B., “Loop Heat Pipe Design, Manufacturing, and Testing – An Industrial Perspective,” ASME 2009 Heat Transfer Summer Conference, San Francisco, CA, July 19-23, 2009.

<sup>2</sup>Ku, Jentung. *Operating characteristics of loop heat pipes*. No. 1999-01-2007. SAE Technical Paper, 1999.

<sup>3</sup>Richard, B., Pellicone, D., and Anderson, W.G., “Loop Heat Pipe Wick Fabrication via Additive Manufacturing,” 48<sup>th</sup> International Conference on Environmental Systems, Albuquerque, New Mexico, July 8-12, 2018.